Circulation Research

ORIGINAL RESEARCH

Infarct Collagen Topography Regulates Fibroblast Fate via p38-Yes-Associated Protein Transcriptional Enhanced Associate Domain Signals

Darrian Bugg, Ross Bretherton, Peter Kim, Emily Olszewski, Abigail Nagle, Austin E. Schumacher, Nick Chu, Jagadambika Gunaje, Cole A. DeForest, Kelly Stevens, Deok-Ho Kim, Jennifer Davis

RATIONALE: Myocardial infarction causes spatial variation in collagen organization and phenotypic diversity in fibroblasts, which regulate the heart's ECM (extracellular matrix). The relationship between collagen structure and fibroblast phenotype is poorly understood but could provide insights regarding the mechanistic basis for myofibroblast heterogeneity in the injured heart.

OBJECTIVE: To investigate the role of collagen organization in cardiac fibroblast fate determination.

METHODS AND RESULTS: Biomimetic topographies were nanofabricated to recapitulate differential collagen organization in the infarcted mouse heart. Here, adult cardiac fibroblasts were freshly isolated and cultured on ECM topographical mimetics for 72 hours. Aligned mimetics caused cardiac fibroblasts to elongate while randomly organized topographies induced circular morphology similar to the disparate myofibroblast morphologies measured in vivo. Alignment cues also induced myofibroblast differentiation, as >60% of fibroblasts formed αSMA (α-smooth muscle actin) stress fibers and expressed myofibroblast-specific ECM genes like Postn (periostin). By contrast, random organization caused 38% of cardiac fibroblasts to express αSMA albeit with downregulated myofibroblast-specific ECM genes. Coupling topographical cues with the profibrotic agonist, TGFβ (transforming growth factor beta), additively upregulated myofibroblast-specific ECM genes independent of topography, but only fibroblasts on flat and randomly oriented mimetics had increased percentages of fibroblasts with αSMA stress fibers. Increased tension sensation at focal adhesions induced myofibroblast differentiation on aligned mimetics. These signals were transduced by p38-YAP (yes-associated protein)-TEAD (transcriptional enhanced associate domain) interactions, in which both p38 and YAP-TEAD (yes-associated protein transcriptional enhanced associate domain) binding were required for myofibroblast differentiation. By contrast, randomly oriented mimetics did not change focal adhesion tension sensation or enrich for p38-YAP-TEAD interactions, which explains the topography-dependent diversity in fibroblast phenotypes observed here.

CONCLUSIONS: Spatial variations in collagen organization regulate cardiac fibroblast phenotype through mechanical activation of p38-YAP-TEAD signaling, which likely contribute to myofibroblast heterogeneity in the infarcted myocardium.

GRAPHIC ABSTRACT: A graphic abstract is available for this article.

Key Words: extracellular matrix ■ fibroblasts ■ fibrosis ■ myocardial infarction ■ nanotechnology

The structural organization of the heart's ECM (extracellular matrix) undergoes extensive remodeling after myocardial infarction (MI), which continues for weeks after injury until the scar matures. Implicit in the remodeling process are changes in ECM composition but also its mechanical properties. These changes are vital to patient outcomes as structurally unstable scars can result in cardiac rupture.[1,2] The association between

Correspondence to: Jennifer Davis, PhD, University of Washington, 850 Republican, No. 343, Seattle, WA 98109, Email jendavis@uw.edu; or Deok-Ho Kim, PhD, Johns Hopkins University, Baltimore, MD, Email deokho@uw.edu

*D.B., R.B., and P.K. contributed equally to this article.

The Data Supplement is available with this article at https://www.ahajournals.org/doi/suppl/10.1161/CIRCRESAHA.119.316162.

For Sources of Funding and Disclosures, see page 1320.

Circulation Research is available at www.ahajournals.org/journal/res

Novelty and Significance

What Is Known?

- Myocardial infarction creates spatially distinct differences in collagen.
- Collagen organization can modulate cell state.
- Heterogeneous cardiac fibroblast cell-state changes contribute to myocardial infarction–induced remodeling of the extracellular matrix.

What New Information Does This Article Contribute?

- Using nanofabricated biomimetics of myocardial infarction–induced changes in collagen alignment, we demonstrated that aligned topographical cues induce cardiac fibroblast-to-myofibroblast state transitions—a maladaptive response.
- Aligned collagen biomimetics increase cardiac fibroblast focal adhesion tension sensation, which is required for topography-dependent cell-state transitions.
- Aligned collagen cues also enrich for p38-YAP (yes-associated protein)-TEAD (transcriptional enhanced associate domain) interactions, and these signals are required for cardiac fibroblast-to-myofibroblast state transitions.

Cardiac fibroblast-to-myofibroblast state transitions are essential for maladaptive extracellular matrix remodeling and scarring after a myocardial infarction. Understanding the signals that regulate this state transition is essential for developing approaches for scar regression—a process that still lacks a tractable therapeutic despite its role in accelerating heart failure. Heterogeneous changes in collagen organization are key events following myocardial infarction, yet previous studies failed to explore how local environmental cues impact these cardiac fibroblast fate changes. This study provides new mechanistic insight into how structural alignment cues from the extracellular matrix regulate cardiac fibroblast fate and function. Through engineering biomimetics of myocardial infarction–dependent differences in regional collagen alignment, we uncovered the novel findings that aligned collagen topography initiates cardiac fibroblast-to-myofibroblast differentiation and that interactions between p38, YAP, and TEAD are essential for transducing these alignment cues into programmed myofibroblast differentiation. Also, we provide the first measurement of topography-dependent focal adhesion tension sensation, which transduces topographical cues upstream of p38, YAP, and TEAD. These results underscore the importance of local physical cues within the extracellular environment in regulating cardiac fibroblast function and suggest that matrix architecture needs to be considered when designing therapeutic strategies.

Nonstandard Abbreviations and Acronyms

αSMA	α-smooth muscle actin
Col1a	collagen 1a
ECM	extracellular matrix
FnEDa	EDa splice variant of fibronectin
FRET	Förster resonance energy transfer
MI	myocardial infarction
NOA76	Norland optical adhesive-76
Postn	periostin
TnC	tenascin C
YAP	yes-associated protein

scar properties and cardiac function has been rigorously investigated,[1–3] but the regulatory mechanisms underlying persistent scar remodeling are still poorly understood.

There are a growing number of studies demonstrating that the ECM's physical properties regulate cell-state transitions.[4–7] Recent findings indicate that the differentiation of resident cardiac fibroblasts into myofibroblasts, which are defined by de novo expression of αSMA (α-smooth muscle actin) and ECM proteins like Postn (periostin), is essential for proper regulation of postinfarct scarring and ECM remodeling.[8–11] Single-cell RNA sequencing studies indicate there is considerable heterogeneity in cardiac fibroblast and myofibroblast populations following MI.[12,13] Because this approach eliminates spatial information, it is unclear how local environmental cues impact this heterogeneity, although previous findings suggest there are temporal and spatial signals that regulate myofibroblast formation following MI.[5,14–16] Indeed, histological evidence suggests that myofibroblast density is low in the scar's core but high in the border zone region.[14,17] Coincidently, regional differences in ECM content and organization are also observed in the remodeled heart after MI, suggesting there is a fundamental relationship between collagen fiber topography and the conversion of cardiac fibroblasts into activated myofibroblasts.[1,18,19] How these spatial variations in matrix topography influence cardiac fibroblast cell state have not been previously explored but could explain (at least in part) some of the fibroblast/myofibroblast heterogeneity and regional variations in cardiac fibroblast phenotype following MI. Moreover, regional ECM structure might underlie bidirectional positive feedback between fibroblasts and the ECM that maintain fibroblasts in an activated myofibroblast

state and subsequently exacerbate maladaptive fibrotic scarring and dysfunction.

The goal of this study was to examine how structural alignment cues from the ECM influence cardiac fibroblast fate. Studying the direct effects of the ECM's structural organization on fibroblast phenotypes in vivo is extremely complicated because the cardiac environment is dynamically changing in both space and time throughout post-MI wound healing and remodeling. Variations in pressure, volume, inflammation, compensatory feedback mechanisms, and alterations in collagen content and structure are happening simultaneously during this process, making it impossible to isolate the effects of collagen organization on cardiac fibroblast biology. To discriminate how spatial heterogeneity in ECM topography in the infarcted heart directly influences cardiac fibroblast phenotype, we engineered biomimetics of collagen alignment cues associated with the border zone and core of the infarct scar. These in vitro mimetics were engineered using nanofabrication techniques and UV light (UV)-curable polymers that recapitulate the stiffness of the infarcted rodent myocardium. By coupling these nanoengineered topographical mimetics with targeted genetic silencing of key signaling pathways, we uncovered that aligned topographical cues increase tension sensation by focal adhesions in cardiac fibroblasts, which in turn induce myofibroblast differentiation programs through boosting p38-YAP (yes-associated protein)-TEAD (transcriptional enhanced associate domain) signaling. By contrast, disorganized topographical mimetics of the infarct scar induced some myofibroblast-like cytoskeletal changes but with reduced EMC gene expression that occurred independent of YAP-TEAD (yes-associated protein transcriptional enhanced associate domain) signaling. Taken together, these data suggest collagen organization differentially regulates cytoskeletal and ECM components of the myofibroblast phenotype, which we postulate contributes to myofibroblast diversity in the infarcted myocardium.

METHODS

The Expanded Methods and Major Resource Sections in the Data Supplement describe all of the experimental approaches and materials used in this study.

All animal experimentation was approved by the University of Washington Institutional Animal Care and Use Committee. Postn lineage reporter mice contain a gene-targeted tamoxifen-inducible Cre cassette in the *Postn* locus ($Postn^{iCre}$) and a conditional membrane-targeted dual fluorescent reporter (mT/mG) in the *Rosa26* locus.[9,10,20] Cardiac fibroblast–specific p38α knockout mice were generated by crossing LoxP-targeted *Mapk14* mice ($p38^{F/F}$) and mice with a tamoxifen-inducible Cre cassette knocked into the *Tcf21* locus ($p38^{F/F}$-$Tcf21^{iCre}$).[10] Cardiac fibroblasts were freshly isolated from the hearts of adult $p38^{F/F}$ mice by enzymatic digestion, expanded, and seeded onto gelatin-coated biomimetics for experimentation. Representative images were selected to depict the mean characteristic of each experimental group.

Statistics

Data are presented as mean±SEM, and *P* values for each comparison are shown within the figure or in Table I in the Data Supplement. GraphPad Prism, versions 7 and 8, and R-statistical package were used for statistical testing, which is described for each experiment in the figure legends and Table I in the Data Supplement. Expanded details are provided in Materials in the Data Supplement.

RESULTS

Regions of Aligned Collagen Are Associated With Higher Myofibroblast Density

After MI, there is widespread spatial heterogeneity in collagen alignment that occurs across species.[18,21,22] Here, spatial variation in collagen fiber orientation was quantified in mice subjected to a surgical model of MI. This procedure elicited infarct sizes of 30% to 40% of the heart and robust scarring of similar magnitude as demonstrated by Picro Sirius Red (PSR) staining of transverse myocardial sections (Figure 1A). At 1 week post-MI, there were regions of highly aligned collagen fibers that run in parallel, as well as areas in which collagen fibers were disorganized and randomly oriented. This observation was confirmed by Col1a (collagen 1a) immunofluorescent imaging (Figure 1B). Here, collagen alignment was analyzed using CurveAlign software,[23,24] which calculated collagen alignment coefficients ranging from zero to 1, where 1 represents fibers that are oriented in parallel and those approaching zero have no directionality. CurveAlign analysis revealed that in the border zone of infarcted mouse hearts, collagen fibers were more highly aligned, whereas fibers in the core of the scar were randomly oriented (Figure 1C). Lineage tracing evidence has demonstrated that myofibroblasts are identified by the expression of Postn and αSMA,[9] and studies before the development of Postn lineage reporter mice had demonstrated higher myofibroblast density in the border zone versus the scar's core.[14,17] To examine whether there are regional differences in myofibroblast density associated with collagen organization, the infarcts described above were performed in Postn lineage reporter mice ($Postn^{iCre}$-mT/mG). To calculate regional myofibroblast cell densities, any area with an average collagen alignment coefficient >0.4 was considered aligned and those <0.4 considered randomly oriented. Within each area, the number of cells that were single positive for Postn ($Postn^+$) and double positive for αSMA and Postn (αSMA^+,$Postn^+$) were counted and normalized to the tissue area encompassing the aligned versus randomly oriented collagen fibers. Both $Postn^+$ and αSMA^+,$Postn^+$ cells were scored, as recent

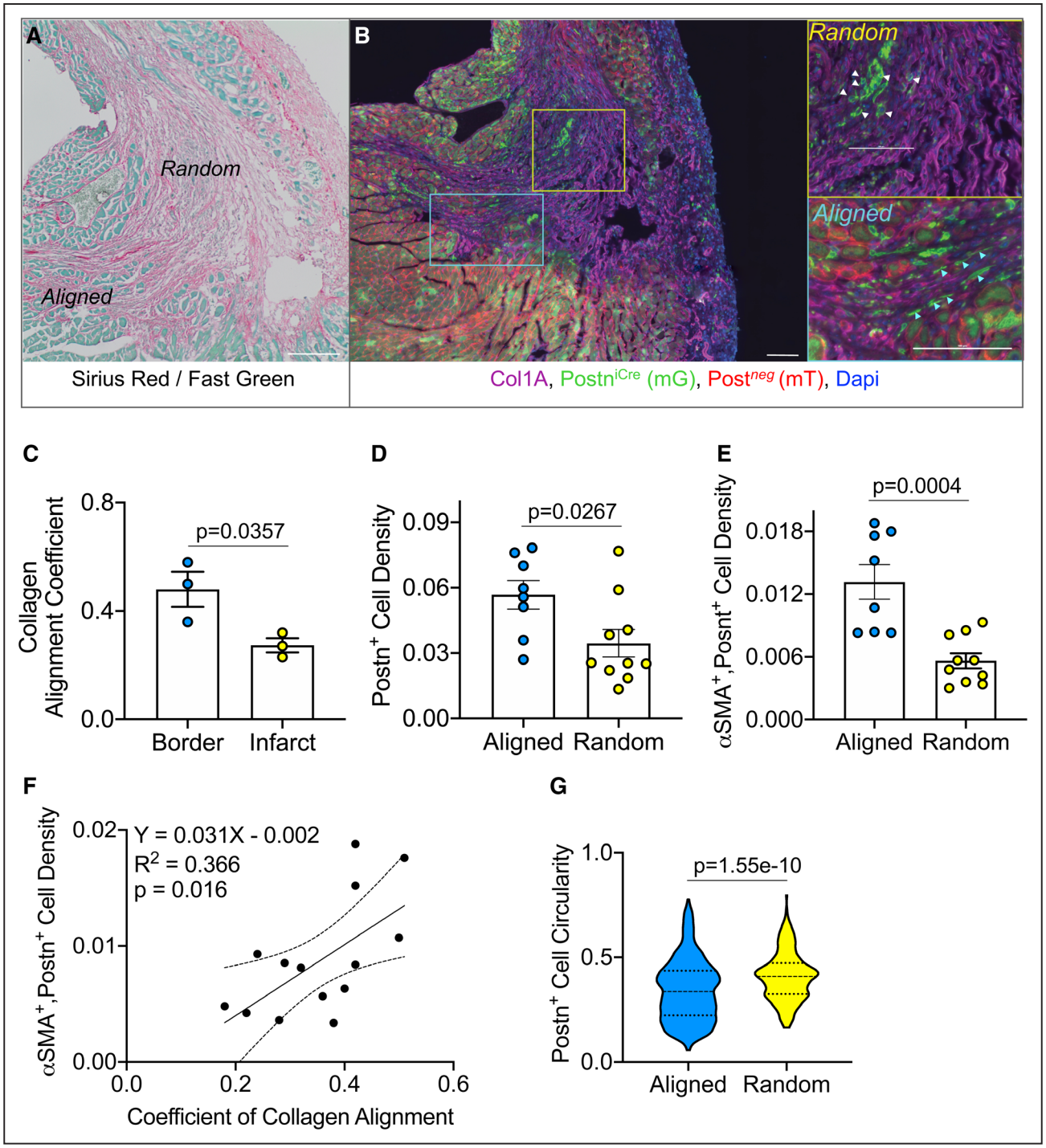

Figure 1. Regions of the infarcted heart with highly aligned collagen are associated with increased myofibroblast density. Representative images of (**A**) Sirius Red-Fast Green and (**B**) collagen I immunofluorescent staining of cardiac sections from infarcted Postn (periostin) lineage reporter mice (Postn^{iCre}-mT/mG). Boxed insets show examples of regions with collagen fibers aligned in parallel vs disorganized (random) orientation. Scale bars=100 μm. **C**, Quantification of the average collagen alignment coefficient in the border zone vs the infarct core. Mann-Whitney *U* test was used, n=3 mice per group with 2 to 4 regions assessed per mouse. **D**, Quantification of the average number of Postn$^+$ cells (stained by eGFP, Postn^{iCre}-mG in **B**) and **E** cells positive for both αSMA (α-smooth muscle actin) and Postn in regions of aligned (coefficients ≥0.4 in **C**, n=8) vs randomly (coefficients <0.4 in **C**, n=10) oriented collagen. Unpaired *t* test was used. Filled circles denote biological replicates. **F**, Linear regression analysis demonstrating the relationship between αSMA$^+$, Postn$^+$ myofibroblast density, and collagen organization where coefficients ≥0.4 equate to a high frequency of aligned collagen fibers. Dashed line=95% CI. **G**, Violin plot of the shape of Postn$^+$ cells in regions of aligned (coefficients ≥0.4 in **C**) vs randomly (coefficients <0.4 in **C**) oriented collagen. Dashed line represents the mean and dotted lines represent the first and third quartiles. Mann-Whitney *U* test was used. Graphs represent mean±SEM. Col1A indicates collagen 1a; and DAPI, 4′,6-diamidino-2-phenylindole.

single-cell RNA sequencing studies have shown transcriptional heterogeneity within the cardiac myofibroblast populations after MI.[12,13] Figure 1D and 1E demonstrates that the density of both Postn$^+$ and αSMA$^+$,Postn$^+$ myofibroblasts is significantly reduced in regions of randomly aligned collagen fibers. Linear regression showed a significant relationship between collagen alignment and αSMA$^+$,Postn$^+$ myofibroblast density, albeit with a small but reliable effect size (Figure 1F). In addition, Postn$^+$ myofibroblast morphology was also significantly different between the two regions (Figure 1G) in which areas with aligned collagen had thin elongated myofibroblasts (Figure 1B, lower right) versus areas of random collagen alignment that had highly circular cells (Figure 1B, upper right). Together, these data suggest that collagen alignment in the infarcted heart is associated with both myofibroblast density and morphology.

Nanoengineered Topographical Mimetics Alter Fibroblast Phenotype

Given the observed relationship between collagen alignment and αSMA$^+$,Postn$^+$ myofibroblast density and morphology, we hypothesized that topographical cues in the ECM regulate cardiac fibroblast phenotype. To test this hypothesis, biomimetics of the aligned and randomly oriented collagen topography were engineered using previously described nanofabrication techniques schematically depicted in Figure 2A.[25] Norland optical adhesive-76 (NOA76)—a polyurethane acrylate material—was used as the biomaterial because its properties robustly recapitulate the elasticity of the infarcted myocardium, which has been quantified in ranges from 50 to 800 kPa in rodents.[26,27] A master pattern film was placed on top of the UV-curing polymer and cured to print the aligned pattern. A randomly oriented collagen pattern was generated by subjecting the aligned pattern to biaxial stretch, ozone treatment, and then shrinking as described previously.[25] The UV-curing polymer was then used to manufacture biomimetic devices of the random collagen topography. Flat (unpatterned) surfaces were developed by using a smooth silicon surface as a master. Flat devices were used to recapitulate standard cell culture surfaces and control for the effects of the polymer's mechanical properties, which has a lower elastic modulus than standard tissue culture plastic or glass.[28] Figure 2B and 2D shows scanning electron microscopy images of a region of the aligned and randomly oriented collagen fibers from sections used for collagen organization analysis (Figure 1) but at the nanoscale. Figure 2C and 2E shows images of the corresponding biomimetic devices. These images were used to evaluate how closely the engineered mimetics of collagen topography recapitulate the average spatial variations in collagen orientation observed in infarcted mice (Figure 2B through 2E, bottom graphs). SEM analysis of synthetic and in vivo collagen fiber nanotopographies showed that 95.5% of collagen fibers in the aligned regions in vivo were within 20° of the major orientation of cells and fibers in that area (Figure 2B). Similarly, 100% of the alignment cues cured into the aligned biomimetic devices were in perfect parallel alignment (Figure 2C). For regions of randomly oriented collagen fibers, 39.8% were within 20° of the major orientation of cells and fibers in that region (Figure 2D). The random biomimetic devices also recapitulated the in vivo frequency of alignment in which only 48.1% of the engineered topographical cues were in parallel alignment (Figure 2E).

To ensure that fibroblasts can be cultured on these biomaterials, mouse embryonic fibroblasts (MEFs) were seeded on flat, aligned, and random devices, and attachment, viability, cell area, and alignment were analyzed 3 days later. MEFs attached with equal affinity to all 3 biomimetics and live-dead staining demonstrated there were no differences in viability between groups (Figure IA and IB in the Data Supplement). Primary cardiac fibroblasts had similar attachment and viability (data not shown), but proliferation was significantly reduced independent of serum concentration on the aligned and random mimetics when compared with flat (Figure 2F). Cellular sensations of local topographical cues have been shown to align cells in parallel to the collagen fibers.[29–31] Here, there were significant topography-dependent effects on mouse embryonic fibroblast (MEF) morphology and cell alignment (Figure IC and ID in the Data Supplement), in which MEFs cultured on aligned mimetics had significantly increased cell areas relative to those on flat surfaces and aligned in parallel with the major orientation of the grooves on the aligned mimetics (Figure ID in the Data Supplement). By contrast, MEFs cultured on random topographies had significantly reduced size and no directionality (Figure IC and ID in the Data Supplement). Similar to MEFs, the actin cytoskeleton of adult cardiac fibroblasts oriented in parallel with the aligned patterns (Figure 2G), and their morphology became elongated and spindly as measured by the increased cell eccentricity (Figure 2H) and smaller geometric extent (Figure 2I). These aligned mimetic-dependent changes in cardiac fibroblast morphology are similar to the morphological changes observed in the Postn$^+$ myofibroblasts in regions of aligned collagen 7 days post-MI (Figure 1G). While we did not observe the same circular morphology on the random patterns that was observed in vivo (Figure 1G), cardiac fibroblast morphology failed to elongate and spread and was more comparable to fibroblasts on flat mimetics. Together, these data highlight that regional variations in topographical cues alter cardiac fibroblast organization and morphology.

Given the significant aligned topography-dependent alterations in cardiac fibroblast morphology and previous evidence demonstrating that collagen organization regulates stem cell phenotypes,[29–31] we postulated that

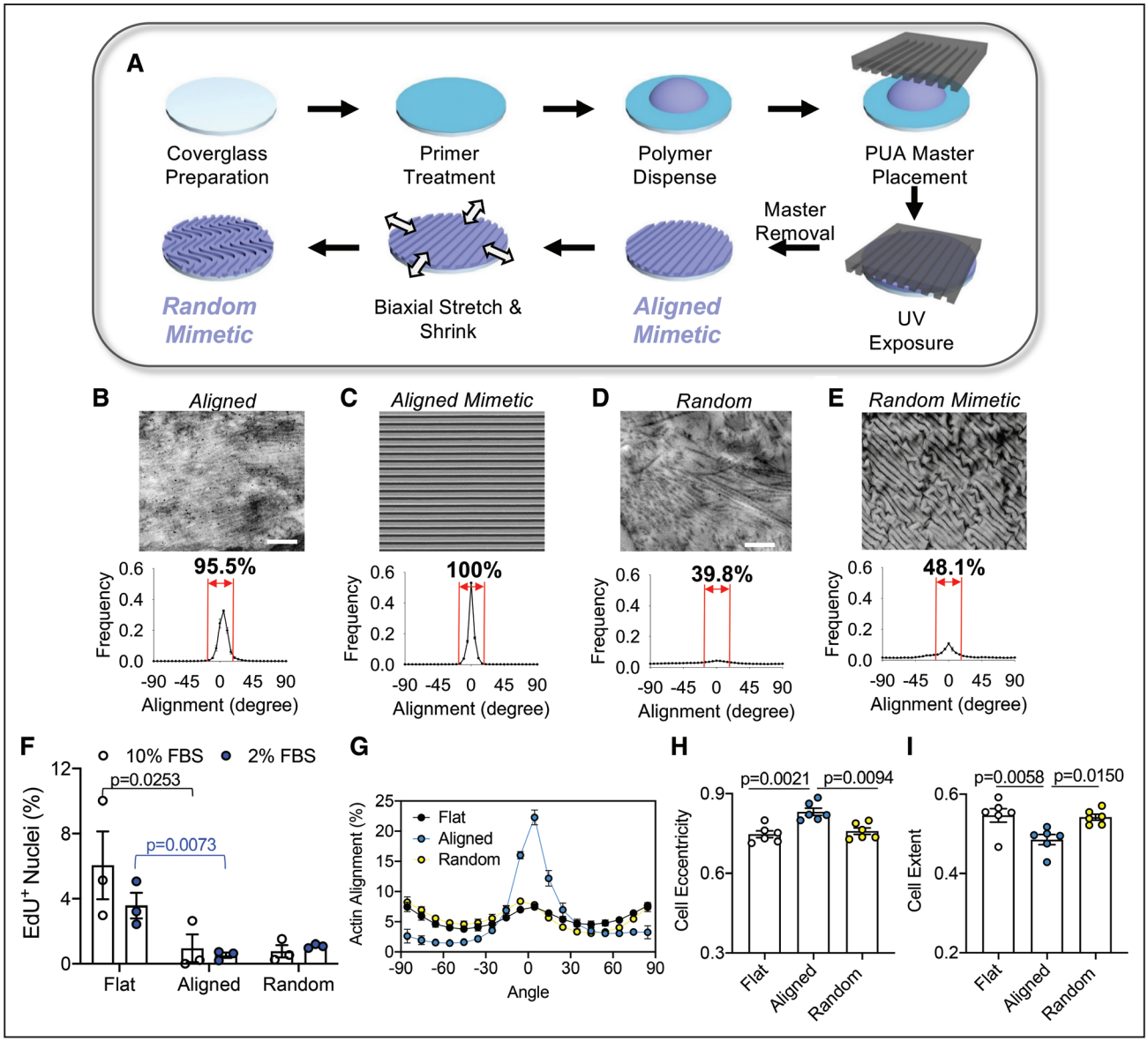

Figure 2. Nanoengineered mimetics of collagen topography alter cardiac fibroblast proliferation and morphology. **A**, Schematics depicting the nanofabrication of each biomimetic. Transmission electron microscopy (TEM) image of (**B**, **top**) aligned and (**D**, **top**) randomly oriented collagen fibers in regions of aligned collagen (coefficients ≥0.4 in Figure 1C) in infarcted mouse hearts, and (**bottom**) the corresponding histogram of the percent collagen fibers aligned within 20° of the major axis. Scanning electron microscopy (SEM) image of nanoengineered (**C**, **top**) aligned and (**E**, **top**) randomly oriented collagen biomimetic and (**bottom**) the corresponding histogram of the percent collagen fiber aligned within 20° of the major axis. **F**, Quantification of EdU+ (5-Ethynyl-2′-deoxyuridine) cardiac fibroblasts cultured on flat, aligned, or random biomimetics in proliferation conditions (10% fetal bovine serum [FBS], n=3 mice, 123–395 cells counted per mouse on flat, 454–904 cells counted per mouse on aligned, and 263–1099 cells counted per mouse on random) and differentiation conditions (2% FBS, n=3 mice, 201–409 cells counted per mouse on flat, 309–480 cells counted per mouse on aligned, and 552–1560 cells counted per mouse on random). Kruskal-Wallis test was performed independently for proliferation and differentiation conditions followed by uncorrected Dunn multiple comparison test between patterns. **G**, Quantification of actin stress fiber alignment (n=3 biological replicates per pattern). Quantification of cell eccentricity (0, circular and 1, a line segment; **H**) and cell extent (higher values=more protrusions; **I**) in cardiac fibroblasts on flat (94–284 cells studied per mouse), aligned (83–767 cells studied per mouse), or random (171–844 cells studied per mouse) biomimetics. Kruskal-Wallis test followed by uncorrected Dunn multiple comparison tests was made between patterns, n=6 biological replicates per group. Graphs represent mean±SEM. PUA indicates polyurethaneurea-vinyl polymer.

cardiac fibroblast cell fate is differentially regulated by aligned and random patterns. Adult cardiac fibroblasts were seeded onto biomimetic platforms for 3 days and then analyzed by immunofluorescent imaging of αSMA+ stress fibers (Figure 3A and 3B), which is a signature of programmed fibroblast-to-myofibroblast differentiation. The percentage of fibroblasts with αSMA+ stress fibers was significantly higher on aligned mimetics in comparison to those with flat and random topographies (Figure 3A and 3B). Notably, random mimetics also had a

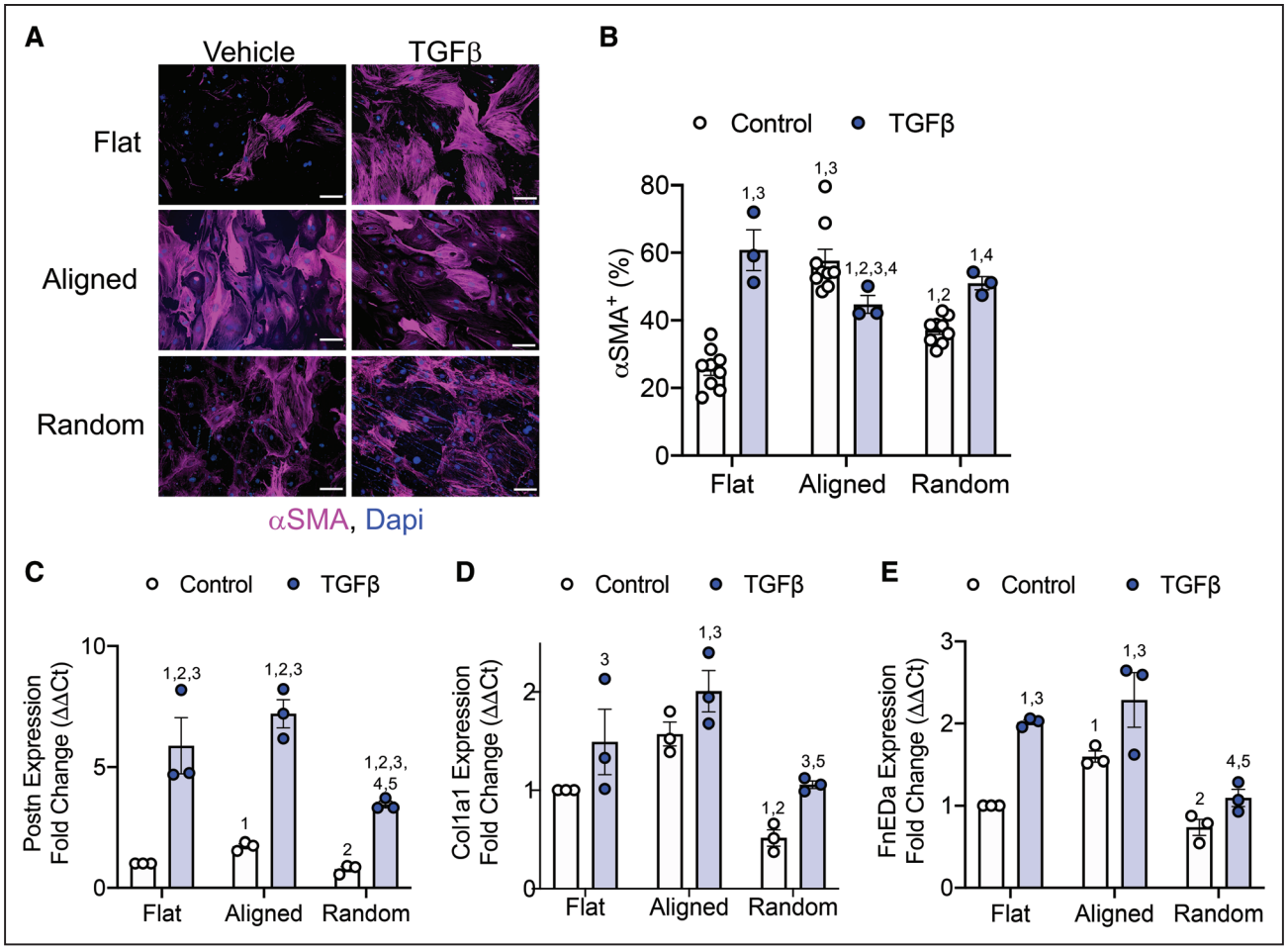

Figure 3. Aligned topographical mimetics promote cardiac fibroblast-to-myofibroblast differentiation.
Immunofluorescent images (**A**) and quantification (**B**) of the percentage of cardiac fibroblasts positive for αSMA (α-smooth muscle actin) stress fibers on flat (177–399 cells studied per mouse), aligned (157–344 cells studied per mouse), and random (220–470 cells studied per mouse) biomimetics with (n=9 mice) and without TGFβ (transforming growth factor beta) (n=3 mice). Scale bars=100 μm. Mixed-effects logistic regression followed by Bonferroni-corrected post hoc comparisons was made between groups. Fold change in Postn (periostin; **C**), Col1a1 (collagen 1a1; **D**), and FnEDa (fibronectin EDa splice variant; **E**) gene expression in fibroblasts on flat, aligned, and random biomimetics with and without TGFβ treatment. Values are calculated using the 2^{-DDCt} method and expressed relative to the flat,control condition; n=3 biological replicates per group. Log-transformed outcome and 2-way ANOVA with the natural log of the variable of interest as the outcome variable and Bonferroni-corrected pairwise comparisons were used for analysis. Graphs represent mean±SEM, 1 vs control,flat, 2 vs control,aligned, 3 vs control,random, 4 vs TGFβ,flat, and 5 vs TGFβ,aligned. DAPI indicates 4′,6-diamidino-2-phenylindole nuclear stain.

significantly higher percentage of the cardiac fibroblast population positive for αSMA stress fibers than those identified on flat surfaces (Figure 3A and 3B). Additional transcriptional markers of the myofibroblast phenotype were analyzed including ECM genes like *Postn* (Figure 3C), *Col1a1* (Figure 3D), and *FnEDa* (Figure 3E). All 3 ECM genes were significantly upregulated in cardiac fibroblasts cultured on aligned patterns when compared with those on flat and random surfaces, but the random mimetic induced no alterations to some ECM genes and a decrease in the expression levels of others, suggesting that collagen organization can differentially regulate myofibroblast-associated cytoskeletal and ECM markers. These analyses were also performed on MEFs and yielded similar findings although the degree of activation was globally depressed (Figure II in the Data Supplement).

After MI, both chemical and physical signals contribute to the regulation of cardiac fibroblast and myofibroblast phenotypes, and so we examined the combinatorial effects of topographical cues and recombinant TGFβ (10 ng/mL)—a key cytokine responsible for fibroblast-to-myofibroblast differentiation and cardiac fibrosis.[4] As expected, TGFβ activated cardiac fibroblasts on flat mimetics as evidenced by the significant increase in cells with αSMA+ stress fibers (Figure 3A and 3B) and upregulation of *Postn* and *FnEDa* gene expression (Figure 3C and 3E). Interestingly, the combination of aligned surfaces and TGFβ decreased the percentage of cardiac fibroblasts positive for αSMA stress fibers (Figure 3A and 3B) but significantly increased of *Postn*, *Col1a1*,

and *FnEDa* gene expression (Figure 3C through 3E). On both flat and random patterns, TGFβ treatment additively increased the percentage of cardiac fibroblasts with αSMA+ stress fibers and ECM gene expression in cardiac fibroblasts (Figure 3A through 3E). While TGFβ increased ECM gene expression in cardiac fibroblasts on random patterns, overall, the response was blunted in comparison to the other mimetics (Figure 3A through 3E). Taken together, these data suggest that TGFβ and ECM topography regulate αSMA stress fiber formation using common intracellular signaling pathways, but independent signals operating in parallel appear to regulate the ECM phenotype.

Focal Adhesions Sense and Transduce Alignment Cues

Previous work has shown that focal adhesions transduce physical signals from topographical cues in the ECM into changes in cellular migration.[32] Hence, we reasoned that collagen alignment mimetics are regulating topography-dependent transitions of fibroblasts into myofibroblasts through focal adhesion signaling. Indeed, immunofluorescent imaging of focal adhesion protein tensin 1 showed that focal adhesion number and size were increased in MEFs cultured on aligned mimetics (Figure 4A through 4C). Similarly, alignment cues increased the expression of TnC (tenascin C), which regulates focal adhesion signaling (Figure 4D).[33] To quantify topography-dependent changes in tension sensation at focal adhesions, cardiac fibroblasts were lentivirally transduced with a Förster resonance energy transfer (FRET)–based tension sensor encoded into the carboxy-tail of vinculin.[34,35] Briefly, the sensor was engineered by separating a Clover-mRuby FRET pair with an elastic element in which FRET efficiency and tension are inversely related. Hence, FRET pairs in close proximity permit high FRET efficiency while tension pulls the FRET pairs apart lowering FRET. Using the sensor's fluorescent output, we observed an increased focal adhesion alignment in cardiac fibroblasts on the aligned biomimetics (Figure 4E and 4F, left). Static FRET measurements in fixed cardiac fibroblasts were significantly decreased in cardiac fibroblasts on aligned mimetics, suggesting that aligned topographical cues cause increased tension sensation at the focal adhesion (Figure 4F). Interestingly, fibroblasts on the random mimetics tended to have higher FRET efficiencies and thus lower tension sensation versus those on flat patterns albeit these values were not statistically different. To determine whether focal adhesion tension sensation is required for mechanically transducing collagen alignment cues into myofibroblast differentiation, shRNA was used to silence tensin 1 expression and the percentage of fibroblasts with αSMA+ stress fibers analyzed. Western blot analysis demonstrated a significant knockdown of Tensin 1 in MEFs when compared with controls (Figure IIIA in the Data Supplement). Loss of tensin 1 significantly lowered baseline fibroblast activation on flat patterns as demonstrated by the reduced percentage of cells with αSMA+ stress fiber expression on flat patterns (Figure 4G). In addition, tensin 1 knockdown blocked aligned pattern-dependent increases in myofibroblast differentiation (Figure 4G), indicating that fibroblasts require focal adhesions to sense and transduce aligned structural cues from the ECM into myofibroblast differentiation.

p38 Transduces Alignment Cues Into Programmed Myofibroblast Differentiation

Previous work in our laboratory has demonstrated that p38 is a nodal point in the signaling network regulating programmed myofibroblast differentiation, as several chemical and mechanical inducers of fibrosis including TGFβ and cyclic stretch require p38 to induce myofibroblast gene transcription.[10] Hence, the role of p38 was examined as an intracellular transducer of topographical cues into programmed myofibroblast differentiation. Adult cardiac fibroblasts were isolated from conditional p38α knockout mice ($p38^{F/F}$) and cultured on flat, aligned, and random topographical mimetics with or without Cre recombinase. Western blot analysis demonstrated that both aligned and random topographies increase p38 expression, which was significantly reduced with Cre-mediated recombination that excises p38α (Figure 5A and 5B). Similarly, aligned mimetics increased p38 activity in MEFs as measured by Western blot for phosphorylated p38 (Figure IIIB in the Data Supplement). Additional evidence of p38 activity was identified by the enhanced localization of p38 in the nucleus of cardiac fibroblasts cultured on the aligned mimetics (Figure 5C). To examine whether p38 is required for pattern-dependent induction of fibroblast-to-myofibroblast differentiation, $p38^{F/F}$ cardiac fibroblasts were cultured on the topographical mimetics with and without recombinant Cre treatment and the percentage of fibroblasts with αSMA+ stress fibers calculated. On both aligned and random patterns, loss of p38 function blocked pattern-dependent activation (Figure 5D). Candidate pathways that might work in parallel or synergistically with p38 were also examined as transducers of these topographical cues into myofibroblast gene expression. Previous findings have shown that dysregulated YAP activity causes spontaneous cardiac fibroblast activation and fibrosis.[36,37] These findings in conjunction with (1) the known role of YAP in regulating the actin cytoskeleton and transmission of topographical cues and (2) data demonstrating that in cancer cells stress induces interactions between YAP transcriptional activator TEAD1 and p38 provided rationale for investigating whether YAP-TEAD-p38 interactions might play a role in this model system.[38,39] Here, cardiac fibroblasts on aligned

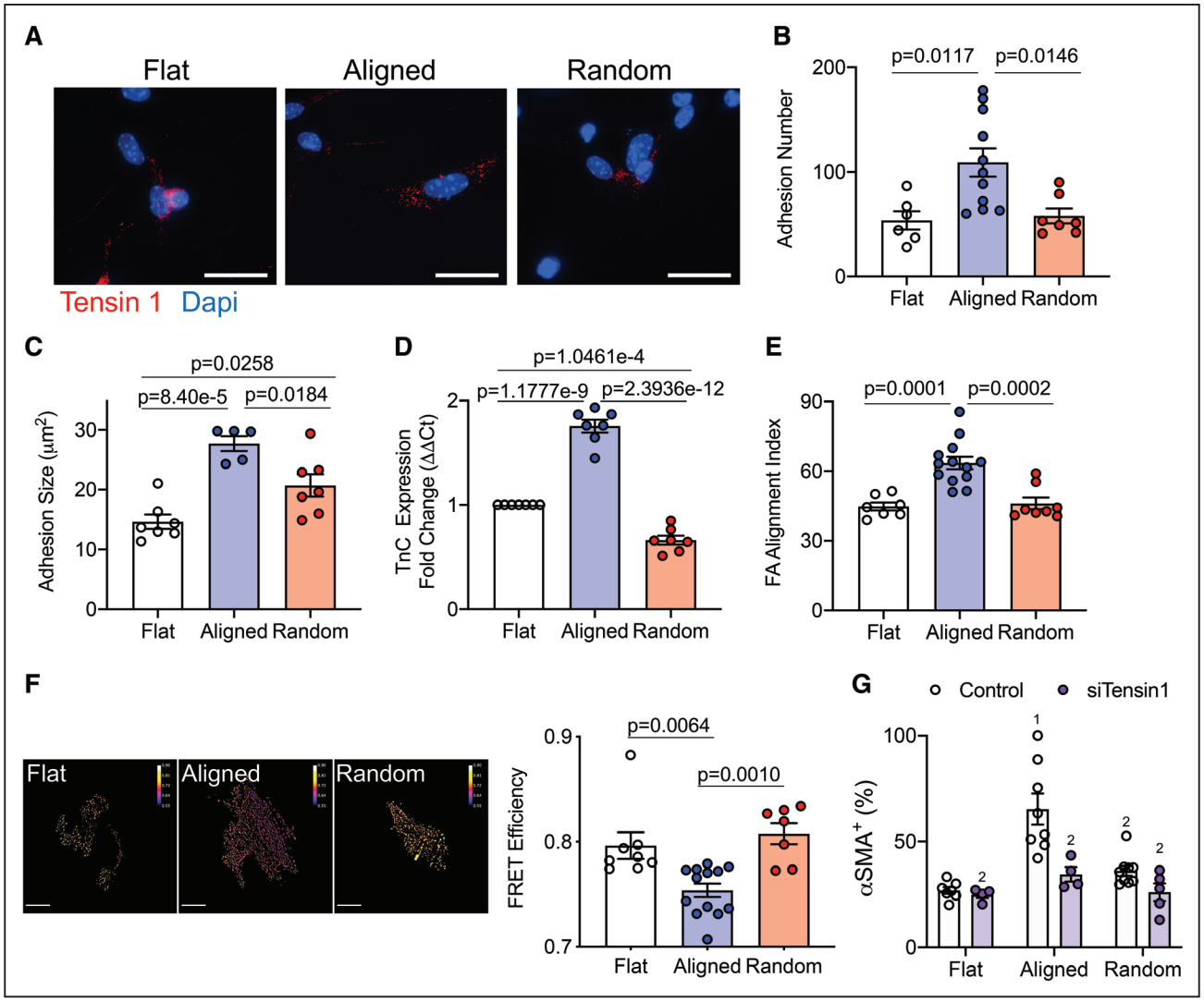

Figure 4. Alignment-induced focal adhesion (FA) and cytoskeletal remodeling is mediated by heightened tension sensation. **A**, Representative immunofluorescent images of mouse embryonic fibroblasts (MEFs) cultured on flat, aligned, and random biomimetics stained with DAPI 4′,6-diamidino-2-phenylindole, (blue) and tensin 1 (red). Scale bar=30 μm. Quantification of tensin 1 positive FA (**B**) number and (**C**) size in MEFs cultured on flat, aligned, and random biomimetics. **D**, Fold change in *TnC* (*tenascin c*) gene expression in cardiac fibroblasts on flat, aligned, and random biomimetics. Values are calculated using the $2^{-\Delta\Delta Ct}$ method and expressed relative to the flat condition. Quantification of (**E**) FA alignment index and (**F**) average Förster resonance energy transfer (FRET) efficiency in cardiac fibroblasts expressing a vinculin tension sensor. **F**, **Left**, Representative image of the acceptor intensity and FRET efficiency of fibroblasts on a flat mimetic. Scale bar=100 μm. Graphs represent mean±SEM, and filled circles denote biological replicates. 1-way ANOVA followed by Tukey post hoc comparisons between groups. **G**, Quantification of the percentage of cardiac fibroblasts positive for αSMA (α-smooth muscle actin) stress fibers when cultured on flat, aligned, and random biomimetics with and without tensin 1 knockdown (siTensin1). Graphs represent mean±SEM, and filled circles denote biological replicates. Mixed-effects logistic regression followed by Bonferroni-corrected post hoc comparisons was used for analysis, 1 vs control,flat and 2 vs control,aligned.

patterns had increased nuclear colocalization of p38 and YAP, as well as p38 and TEAD (Figure 5E and 5F). To verify the interaction between p38, YAP, and TEAD, lysates were collected from cardiac fibroblasts cultured on flat, aligned, and random mimetics and a phosphorylated p38 antibody used to immunoprecipitate proteins bound to activated p38. Western blot analysis of immunoprecipitates demonstrated that on all 3 patterns, p38, YAP, and TEAD are complexed together (Figure 5G), but there is an enrichment of p38-YAP-TEAD binding in lysates from fibroblasts on aligned mimetics when compared with flat or random surfaces (Figure 5H and 5I). Similar results were seen in MEFs in which YAP was immunoprecipitated by a phosphorylated p38 antibody only in lysates from the aligned pattern (Figure IIIC in the Data Supplement). On the random mimetics, phosphorylated p38 still immunoprecipitated YAP and TEAD in cardiac fibroblasts lysates, but the level of binding was significantly reduced when normalized to the input (Figure 5G through 5I). These data suggest that collagen organization differentially regulates p38-YAP-TEAD interactions.

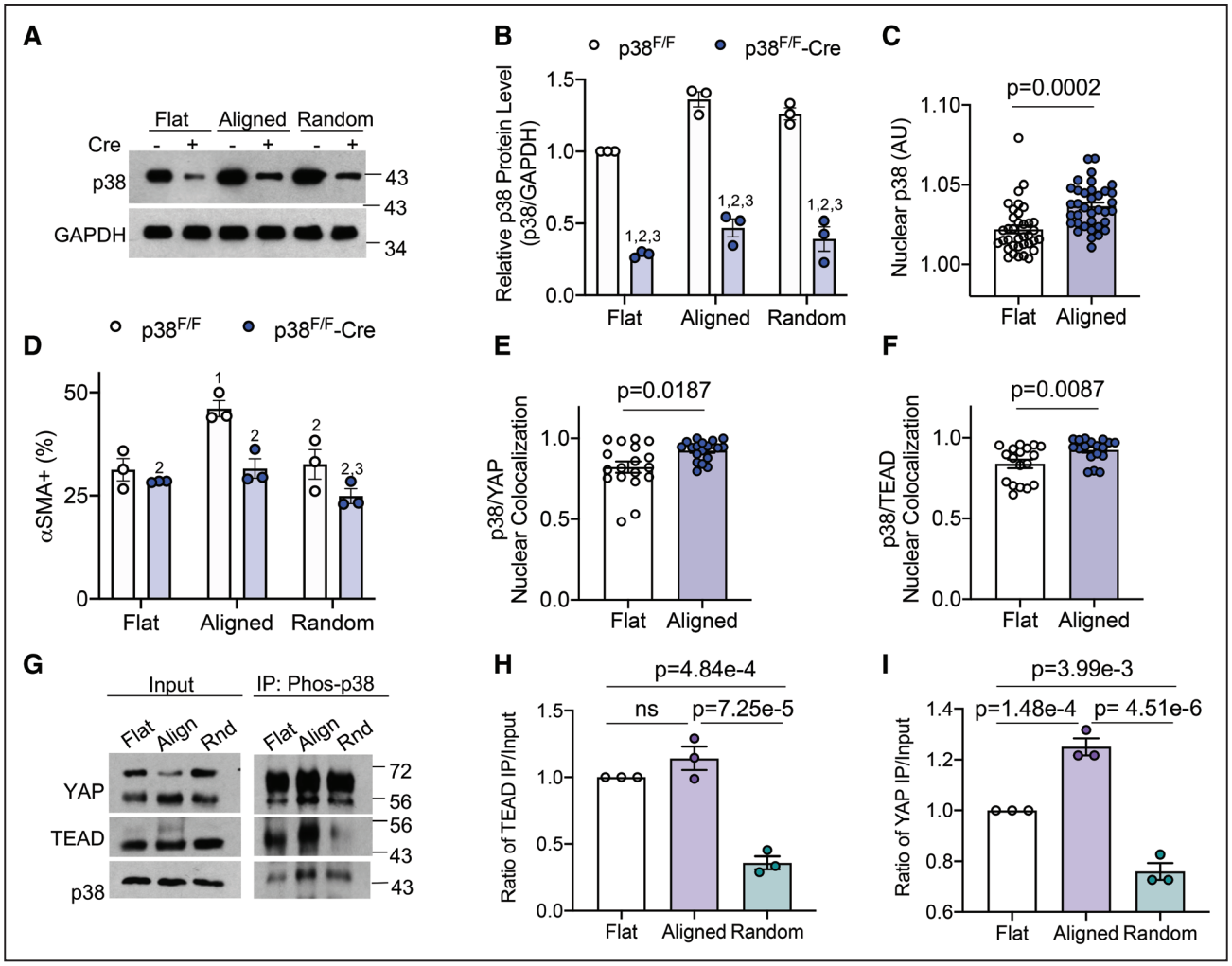

Figure 5. p38 is required for alignment-induced myofibroblast differentiation and colocalization of YAP (yes-associated protein) and TEAD (transcriptional enhanced associate domain).

Representative Western blot (**A**) and densitometry analysis (**B**) of p38 and GAPDH expression in cardiac fibroblasts cultured on flat, aligned, and random biomimetics with (+) and without (–) Cre. Graphs represent mean±SEM; n=3 biological replicates; log-transformed outcome and 2-way ANOVA with the natural log of the variable of interest as the outcome variable and Bonferroni-corrected pairwise comparisons were used for analysis: 1 vs $p38^{F/F}$,flat, 2 vs $p38^{F/F}$,aligned, and 3 vs $p38^{F/F}$,random. **C**, Quantification of intensity of p38 staining in the nucleus in cardiac fibroblasts cultured on flat and aligned biomimetics. Graphs represent mean±SEM; n=36 biological replicates per group. Mann-Whitney *U* test was used. **D**, Quantification of the percentage of $p38^{F/F}$ cardiac fibroblasts positive for αSMA (α-smooth muscle actin) stress fibers on flat (231–451 cells studied per mouse within each condition), aligned (186–279 cells studied per mouse within each condition), and random biomimetics (253–380 cells studied per mouse within each condition) with and without Cre; n=3 biological replicates; and mixed-effects logistic regression followed by Bonferroni-corrected post hoc comparisons were made between groups: 1 vs $p38^{F/F}$,flat, 2 vs $p38^{F/F}$,aligned, and 3 vs $p38^{F/F}$,random. **E**, Quantification of the nuclear colocalization of p38 and YAP and (**F**) p38 and TEAD in cardiac fibroblasts on flat and aligned biomimetics. Graphs represent mean±SEM; n=36 biological replicates per group. Mann-Whitney *U* test was used. **G**, Representative Western blot of lysates (input) and phosphorylated p38 immunoprecipated proteins (IP; Phos-p38) from these inputs, which were derived from cardiac fibroblasts on flat, aligned (align), and random (Rnd) biomimetics. **H**, Quantification of the ratio of phospho-p38 immunoprecipitated TEAD to TEAD-input and (**I**) YAP to YAP-input. Here, log-transformed outcome analysis and 1-way ANOVA with the natural log of the variable of interest as the outcome variable and Bonferroni-corrected pairwise comparisons were used for analysis. All graphs represent mean±SEM; filled circles denote biological replicates. ns indicates not significant.

p38-YAP-TEAD Signaling Underlies Topography-Dependent Regulation of Fibroblast Phenotype

To determine whether there are both p38 and topography-dependent effects on YAP activity, Western blot was used to analyze YAP expression and phosphorylation status in $p38^{F/F}$ cardiac fibroblasts with and without Cre (Figure 6A). This experiment revealed a pattern-dependent increase in YAP protein expression that was significantly reduced in conditional p38 knockout cardiac fibroblasts (+Cre lanes; Figure 6A and 6B). No changes in YAP gene expression were detected with loss of p38 (Figure 6C), suggesting that p38 is required for post-translational YAP stabilization. YAP nuclear-cytoplasmic shuttling was also examined in this context by 2

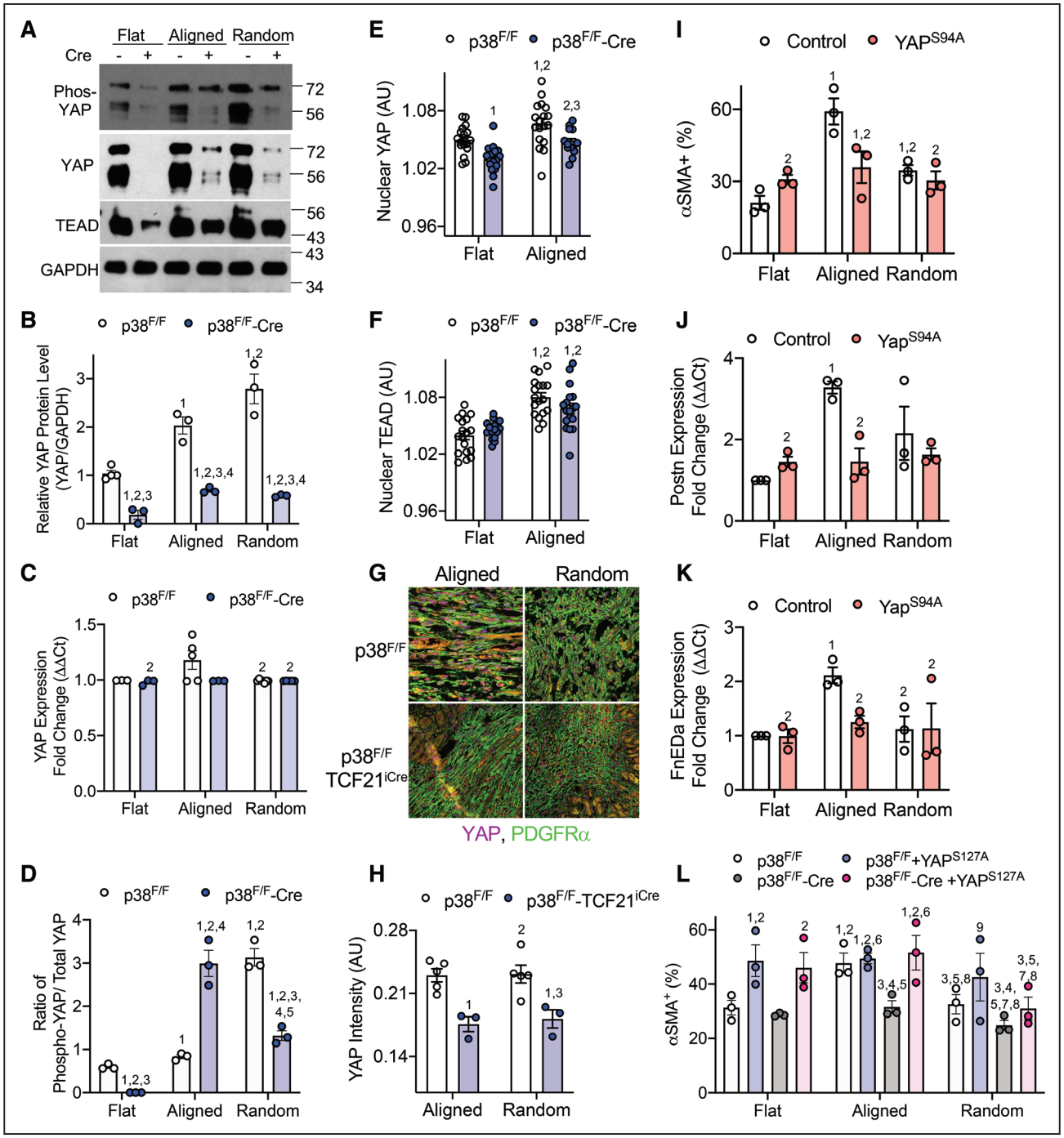

Figure 6. p38-YAP (yes-associated protein)-TEAD (transcriptional enhanced associate domain) interactions are necessary for alignment-induced myofibroblast differentiation.

A, Representative Western blot of phosphorylated YAP (phos-YAP), total YAP, pan TEAD, and GAPDH expression. Here, GAPDH served as a loading control. **B**, Densitometry analysis of YAP protein levels normalized to GAPDH. **C**, Change in YAP gene expression in cardiac fibroblasts on flat, aligned, and random biomimetics with (+) and without (–) Cre. Values are calculated using the $2^{-\Delta\Delta Ct}$ method and expressed relative to flat,$p38^{F/F}$ condition. **D**, Quantification of the ratio of phosphorylated YAP to total YAP protein levels in cardiac fibroblasts on flat, aligned, and random biomimetics with (+) and without (–) Cre. **B**, **C**, and **D**, Graphs represent mean±SEM; n=3 biological replicates; log-transformed outcome and 2-way ANOVA with the natural log of the variable of interest as the outcome variable and Bonferroni-corrected pairwise comparisons were used for analysis where 1 vs $p38^{F/F}$,flat, 2 vs $p38^{F/F}$,aligned, 3 vs $p38^{F/F}$,random, 4 vs $p38^{F/F}$-Cre,flat, and 5 vs $p38^{F/F}$-Cre,aligned. Quantification of intensity of (**E**) YAP and (**F**) TEAD staining in the nucleus of $p38^{F/F}$ cardiac fibroblasts cultured on flat and aligned biomimetics with and without Cre. Graphs represent mean±SEM, n=18 except for the aligned-$p38^{F/F}$-Cre group in **E** where n=14. Two-way ANOVA and Tukey post hoc comparisons were made between groups, 1 vs flat,$p38^{F/F}$, 2 vs flat,$p38^{F/F}$-Cre, 3 vs aligned,$p38^{F/F}$. **G**, Representative images and (**H**) quantification of nuclear YAP staining intensity (purple) in PDGFRα^{+} (platelet derived growth factor receptor alpha) cardiac fibroblasts (green) in cardiac tissue sections from infarcted $p38^{F/F}$ and $p38^{F/F}$-Tcf21^{iCre} mice. Nuclei are stained with Hoechst, and staining intensity was subclassified by regions of aligned (coefficients ≥0.4 in Figure 1C) vs random (coefficients <0.4 in Figure 1C) collagen organization. (*Continued*)

independent assays: Western blot for phosphorylated YAP (Figure 6A and 6D), which keeps YAP cytosolic, and immunofluorescent imaging of YAP subcellular localization (Figure 6E). While aligned mimetics increased YAP protein expression, the levels of phosphorylated-to-total YAP were not statistically different from flat controls (Figure 6A and 6D). On the random patterns, levels of phosphorylated-to-total YAP were significantly elevated suggesting that random collagen alignment promotes cytosolic YAP retention (Figure 6A and 6D). Notably, there was a p38-mediated decrease in phosphorylated YAP in all groups, which we believe is simply a function of the reduction in total YAP protein expression (Figure 6A). However, on aligned surfaces, the ratio of phosphorylated-to-total YAP was higher in conditional p38 knockouts ($p38^{F/F}$+Cre; Figure 6D), suggesting that the limited amount of YAP in p38 knockouts remains cytosolic. Consistent with phosphorylated-to-total YAP ratios, nuclear YAP was increased in cardiac fibroblasts on aligned mimetics, which was significantly decreased with loss of p38 (Figure 6E). Deletion of p38 also decreased nuclear YAP on the flat mimetic likely because YAP requires p38 function for protein stability (Figure 6A through 6C). Since TEAD was also in complex with YAP and p38, nuclear TEAD levels were assessed, and unlike YAP, there were no significant effects of p38 loss of function on nuclear TEAD (Figure 6F). There was, however, a significant enhancement in nuclear TEAD localization on aligned patterns (Figure 6F). To determine whether collagen alignment and p38 alter YAP nuclear localization in vivo, cardiac tissue sections from wild-type ($p38^{F/F}$) and cardiac fibroblast–specific p38α knockout mice ($p38^{F/F}$+$Tcf21^{iCre}$) were examined using immunofluorescent imaging of cardiac sections 1 week after MI. Here, the intensity of nuclear YAP was measured in resident cardiac fibroblasts that were identified by PDGFRα (platelet derived growth factor receptor alpha) staining (Figure 6G). Using collagen alignment coefficients described in Figure 1C, nuclear YAP intensity was quantified in regions of aligned versus random collagen orientation (Figure 6G and 6H). There were no significant differences in nuclear YAP intensity in regions of aligned versus randomly oriented collagen, but consistent with in vitro findings, loss of p38 significantly reduced nuclear YAP intensity (Figure 6G and 6H).

To determine whether YAP is required for alignment-dependent myofibroblast differentiation, cardiac fibroblasts were transfected with a dominant-negative YAP (YAP^{S94A}) that is deficient in the TEAD-binding site.[40] Expression of dominant-negative YAP^{S94A} blocked myofibroblast differentiation induced by the aligned mimetics as evidenced by the drop in cardiac fibroblasts with αSMA$^+$ stress fibers (Figure 6I) and upregulated myofibroblast ECM genes like *Postn* and *FnEDa* (Figure 6J and 6K). Cardiac fibroblasts cultured on random mimetics, which induce a mild but significant αSMA$^+$ stress fiber phenotype and no change in ECM gene expression, were also rescued by YAP^{S94A} expression. In the opposing gain-of-function experiments, overexpression of constitutively active YAP (YAP^{S127A}) in cardiac fibroblasts demonstrated that nuclear YAP activity is sufficient to induce αSMA$^+$ stress fiber phenotype on flat and random patterns, but it failed to additively increase the number of myofibroblasts on the aligned mimetics (Figure 6L). Interestingly, a significant percentage of conditional p38 knockout cardiac fibroblasts, which are refractory to alignment-induced myofibroblast differentiation ($p38^{F/F}$+Cre; Figure 6L), spontaneously developed an αSMA$^+$ stress fiber phenotype with the expression of constitutively active YAP independent of alignment cues, suggesting that YAP signaling mechanisms are downstream of p38 activity (Figure 6L). Notably, the random mimetic tempered YAP^{S127A}-mediated differentiation (Figure 6L) suggesting that disorganized topographical cues trigger alternative signaling pathways that partially repress the myofibroblast phenotype.

DISCUSSION

The spatial heterogeneity of collagen fiber organization in the infarcted myocardium broadly impacts myocardial biomechanics[18,41] but also provides extracellular mechanical cues that locally regulate cardiac fibroblast fate.[42] Since fibroblasts in their differentiated myofibroblast

Figure 6 Continued. Graphs represent mean±SEM; n=3 to 5 biological replicates as denoted by the circles; 2-way ANOVA and Tukey post hoc comparisons were made between groups; 1 vs flat,$p38^{F/F}$, 2 vs flat,$p38^{F/F}$-Cre, and 3 vs aligned,$p38^{F/F}$. **I**, Quantification of the percentage of fibroblasts positive for αSMA (α-smooth muscle actin) stress fibers on flat (177–504 cells studied per mouse), aligned (310–604 cells studied per mouse), and random biomimetics (320–358 cells studied per mouse) with and without dominant-negative YAP (YAP^{S94A}) expression. Mixed-effects logistic regression followed by Bonferroni-corrected post hoc comparisons was made between groups. Fold change in (**J**) Postn (periostin) and (**K**) FnEDa (fibronectin EDa splice variant) gene expression in cardiac fibroblasts on flat, aligned, and random biomimetics with and without dominant-negative YAP (YAP^{S94A}) expression. Values are calculated using the $2^{-\Delta\Delta Ct}$ method and expressed relative to the flat,control condition. Here, log-transformed outcome and 2-way ANOVA with the natural log of the variable of interest as the outcome variable and Bonferroni-corrected pairwise comparisons were used for analysis. **I**–**K**, Graphs represent mean±SEM and statistically significant comparisons defined as 1 vs flat,control, 2 vs aligned,control, and 3 vs random,control. **L**, Quantification of the percentage of fibroblasts positive for αSMA stress fibers on flat (202–279 cells studied per mouse), aligned (310–604 cells studied per mouse), and random (204–402 cells studied per mouse) biomimetics with and without constitutively active YAP (YAP^{S127A}) expression. Graphs represent mean±SEM; n=3 biological replicates; mixed-effects logistic regression followed by Bonferroni-corrected post hoc comparisons was made between groups where 1 vs flat,$p38^{F/F}$, 2 vs flat,$p38^{F/F}$-Cre, 3 vs flat,$p38^{F/F}$,YAP^{S127A}, 4 vs flat,$p38^{F/F}$-Cre,YAP^{S127A}, 5 vs aligned,$p38^{F/F}$, 6 vs aligned,$p38^{F/F}$-Cre, 7 vs aligned,$p38^{F/F}$,YAP^{S127A}, 8 vs aligned,$p38^{F/F}$-Cre,YAP^{S127A}, and 9 vs random,$p38^{F/F}$-Cre; only significant relationships are shown.

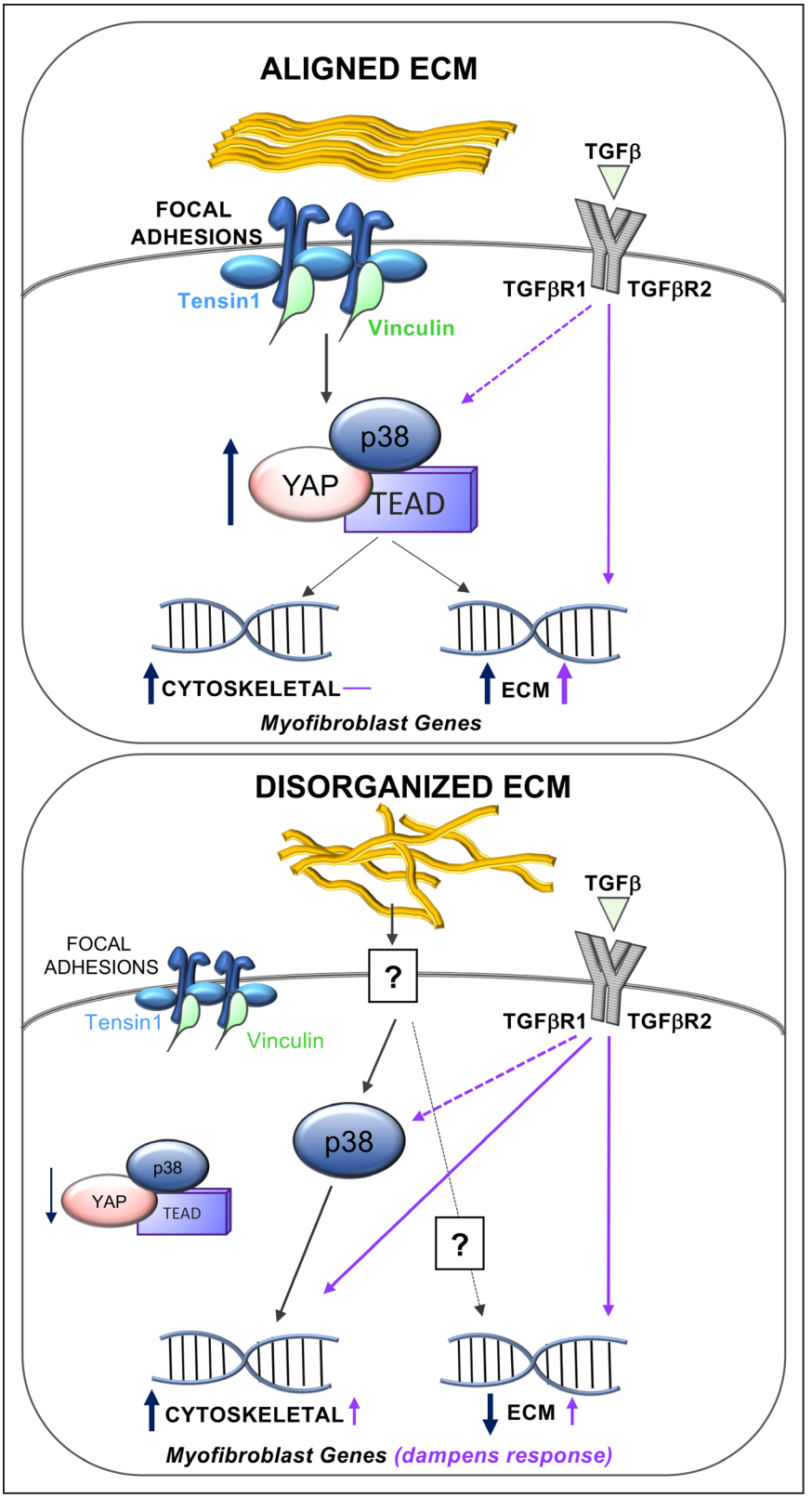

Figure 7. Signaling model of ECM (extracellular matrix) topography–dependent regulation of programmed cardiac myofibroblast differentiation. Dashed arrow represents previously identified interactions between signaling nodes. YAP indicates yes-associated protein. TEAD, transcriptional enhanced associate domain; and TGFb transforming growth factor beta.

state deposit and remodel the ECM during cardiac disease and injury, we aimed to understand how fibroblasts sense and integrate physical signals from the microenvironment into their fate decisions. Figure 7 models the signaling and functional gene expression changes in response to differential topographical cues. The data presented support our conclusion that aligned collagen organization induces myofibroblast differentiation, given ≈60% of the population had αSMA$^+$ stress fibers and a concomitant upregulation in myofibroblast-specific ECM

genes like *Postn* and *FnEDa*.[4,6] This differentiation program was put into motion by increased tension sensation at focal adhesions (Figure 4F), which was transduced into myofibroblast gene expression via an enrichment of p38-YAP-TEAD interactions and activity. p38 stood out as the nodal transducer of the aligned topographical cues because it was required to (1) elicit myofibroblast differentiation (Figure 5) and (2) posttranslationally stabilize and enrich for nuclear YAP (Figure 6). Notably, YAP on its own was both necessary and sufficient for inducing myofibroblast gene programs (Figure 6). By contrast, disorganized ECM, which was mimicked by the random patterns, induced a mild cytoskeletal phenotype akin to myofibroblasts but with downregulated myofibroblast-specific ECM genes (Figure 7). The mild cytoskeletal phenotype was not induced by a change in focal adhesion tension sensation, but it did require p38 signaling (Figure 5). In addition, loss of YAP's ability to bind TEAD failed to block the mild cytoskeletal phenotype suggesting that p38-YAP-TEAD interactions are not transducing signals from disorganized ECM topography. Yet unknown is the identity of receptors and ligands upstream of p38 that contribute to these outcomes and how this pathway is downregulating matrix gene expression.

The coupling of both physical and chemical cues was also studied by treating cardiac fibroblasts cultured on our topographical mimetics with TGFβ. Here, TGFβ failed to additively increase the cytoskeletal myofibroblast phenotype suggesting that aligned structural cues and TGFβ converge on a common intracellular pathway that regulates the cytoskeletal phenotype. Given previous work demonstrating that TGFβ requires p38 to induce myofibroblast differentiation,[8,10] we postulated in our model that both alignment signaling and TGFβ are converging on p38 to elicit the cytoskeletal remodeling (Figure 7). TGFβ additively increased the expression of myofibroblast-specific ECM genes suggesting there is a TGFβ-sensitive pathway not regulated by p38-YAP-TEAD signaling that boosts the ECM component of the myofibroblast phenotype in parallel. Possible candidate factors are small mothers against decapentaplegic (SMAD) 2 and 3, which were not studied here but shown previously to regulate cardiac fibroblast-to-myofibroblast differentiation in vivo.[43,44] Interestingly, cardiac fibroblasts on random mimetics responded to TGFβ in which both myofibroblast-linked cytoskeletal and ECM components were upregulated, but the magnitude of the overall response was dampened relative to the levels achieved on both flat and aligned topographical mimetics (Figure 3).

The transition from ordered to disorganized collagen structure is a hallmark of disease progression and wound healing that transcends tissues and disease etiologies as these organizational changes are also observed in tumor microenvironments.[29,45–48] Here, we observed that the infarcted mouse myocardium has regional variation in collagen organization in which the scar's core has more disorganized and randomly oriented collagen fibers versus the border zone, which has more fibers aligned in parallel (Figure 1A through 1C). Similar regional variations in collagen topography have been shown in rat MI models.[41,46,49] Interestingly, chronic MI in pig, dog, and human also display regional variation in collagen topography but with disordered fibers in the border zone and highly aligned collagen structure in the core of the infarct scar.[41,46,49] Despite these differences in the spatial location of aligned collagen fibers, higher myofibroblast density has been observed in regions where collagen fibers are in parallel alignment in several species,[14,17] as observed and quantified here in our mouse MI model (Figure 1D through 1F). These in vivo findings further support that aligned ECM topography is a positive regulator of programmed myofibroblast differentiation. This regional variation in collagen alignment persists for weeks and even months after infarct and is consistently prevalent in an injured or diseased tissue,[41,46] suggesting that aligned collagen organization positively reinforces the maintenance of an activated fibroblast state. A recent study using single-cell RNA sequencing and lineage tracing approaches demonstrated that fibroblasts undergo 2 cell-state changes as the heart repairs and remodels over a 4-week period after MI.[50] It is unclear how regional heterogeneity in collagen structure impacts the second osteogeneic/cartilage cell-state transition, but these topographical mimetics could be utilized in long-term cultures in combination with profibrotic molecules to further investigate time-dependent regulation of fibroblast fate and function. Moreover, the sensitivity of cardiac fibroblasts to these topographical cues may help explain, in part, fibroblast heterogeneity within an injured tissue,[12,13,45] highlighting the need to examine relationships between spatial location and cell state, particularly in organs with anisotropic mechanical properties like the heart.[30,51,52]

Fibroblasts have been established as mechanically sensitive cells, but how different physical cues are sensed and transduced into cell-state changes is poorly defined.[6,53,54] Tension sensation measured in vinculin demonstrated that there was higher tension at focal adhesions in cardiac fibroblasts cultured on aligned mimetics when compared with other surfaces, which we believe underlie an adaptive growth in focal adhesion number and size (Figure 4). The intracellular signal transducers uncovered the unexpected finding that aligned topographical cues initiated p38-YAP-TEAD interactions (Figure 6). Independently, p38 and YAP were required for alignment-dependent myofibroblast differentiation (Figures 5 and 6), and because p38 is required for YAP protein stabilization (Figure 6), the pathway was modeled with p38-YAP-TEAD complex as the transducer of aligned ECM cues (Figure 7). Notably, after MI cardiac fibroblast–specific p38 knockouts had reduced YAP staining in resident cardiac

fibroblasts suggesting that p38-dependent regulation of YAP protein stability holds true in vivo (Figure 6G and 6H). Previous studies have identified YAP's involvement in transducing mechanical cues into cell fate change and found that unrestrained YAP transcriptional activity by loss of Lats1/2 (large tumor suppressor kinase)-mediated repression spontaneously induces cardiac fibroblast-to-myofibroblast differentiation and fulminant fibrosis in mice.[36,55,56] Our findings that overexpression of a constitutively nuclear YAP is sufficient to induce a myofibroblast phenotype further support these findings (Figure 6L). The novel findings presented here include the following: (1) YAP-mediated myofibroblast transcriptional activity acts downstream of p38 and (2) YAP is posttranslationally regulated by p38 independent of the Lats1/2-*Hippo* pathway.[36] Moreover, these topography-induced interactions between p38-YAP-TEAD extend the network of chemical and mechanical signals that converge on p38 MAPK to induce a myofibroblast phenotype.[4,10] The requirement for p38 MAPK signaling in programmed myofibroblast differentiation and scar formation has been verified in vivo in a mouse model with cardiac fibroblast–specific loss of p38α,[10] but until now, it was unclear whether p38 MAPK signaling also transduces structural cues from the ECM. In cancer cells, hyperosmotic stress, which compresses a cell, induces p38-TEAD interactions that pulls TEAD out of the nucleus causing cytosolic retention of YAP and inhibition of YAP-TEAD transcription.[38] While tension sensation at the focal adhesions in fibroblasts on the random mimetics was not statistically different from flat, the lower FRET efficiency and cellular morphology indicate disorganized topographical cues in vitro and in vivo compress the cell similar to hyperosmolarity (Figures 1G, 2H, and 2I). Indeed, YAP phosphorylation was increased by random mimetics suggesting there is more YAP in the cytosol (Figure 6D) but with reduced TEAD-p38 interactions, which should reduce myofibroblast gene transcription (Figure 5G through 5I). The exact opposite occurred in cardiac fibroblasts on the aligned mimetics in which there was increased tension at the focal adhesions and enhanced colocalization of p38-YAP-TEAD in the nucleus (Figure 5). Taken together, these data suggest that p38-YAP-TEAD interactions are highly sensitive to physical signals that stretch or compress a cell. Unfortunately, we were unable to resolve collagen topography–dependent effects on YAP subcellular localization in cardiac fibroblasts in infarcted mouse hearts, possibly due to resolution limitations our imaging approach (Figure 6G and 6H).

Collectively, this study provides new insights into the mechanisms by which fibroblasts respond to regional heterogeneity in collagen fiber organization associated with MI. By engineering biomimetics that recapitulate the heterogenous organization of the heart's ECM and combining them with genetic engineering, this study added new nodes to the network regulating cardiac fibroblast fate during post-MI remodeling. These results stress the importance of investigating context-dependent fibroblast function especially pertaining to spatial location and local physical cues within the extracellular environment, and they suggest that redesigning matrix architecture could be used as therapeutic strategy to prevent the maintenance of maladaptive fibrotic cell states.

ARTICLE INFORMATION

Received October 9, 2019; revision received August 26, 2020; accepted September 3, 2020.

Affiliations

Bioengineering (R.B., P.K., E.O., A.N., N.C., C.A.D., K.S., J.D.), Pathology (D.B., J.G., K.S., J.D.), Institute for Stem Cell and Regenerative Medicine (C.A.D., K.S., J.D.), Center for Cardiovascular Biology (D.B., R.B., E.O., A.N., J.G., K.S., J.D.), Chemical Engineering (C.A.D.), and Biostatistics (A.E.S.), University of Washington, Seattle. Biomedical Engineering, Johns Hopkins University, Baltimore, MD (D.-H.K.). Medicine, Johns Hopkins School of Medicine, Baltimore, MD (D.-H.K.).

Acknowledgments

R. Bretherton, E. Olszewski, P. Kim, A. Nagel, N. Chu, D. Bugg, and J. Gunaje conducted all of the experiments, which were designed by J. Davis and D.-H. Kim. R. Bretherton, D. Bugg, E. Olszewski, A. Nagel, A.E. Schumacher, K. Stevens, C.A. DeForest, P. Kim, D.-H. Kim, and J. Davis contributed to writing the manuscript.

Sources of Funding

This work was supported by grants from the National Institutes of Health for J. Davis (HL141187 and HL142624) and D.-H. Kim (EB028094, HL135143, and HL146436), K. Stevens (DP2HL137188), and E. Olszewski (HL151017), as well as a Graduate Research Fellowship from the National Science Foundation for R. Bretherton (2018261576).

Disclosures

D.-H. Kim is a scientific founder and equity holder of NanoSurface Biomedical, Inc. The other authors report no conflicts.

Supplemental Materials

Figures I–III
Table I
Expanded Methods
References[6,8–10,20,23–25,34–35,52,57–63]

REFERENCES

1. Richardson WJ, Clarke SA, Quinn TA, Holmes JW. Physiological implications of myocardial scar structure. *Compr Physiol.* 2015;5:1877–1909. doi: 10.1002/cphy.c140067
2. Rog-Zielinska EA, Norris RA, Kohl P, Markwald R. The living scar–cardiac fibroblasts and the injured heart. *Trends Mol Med.* 2016;22:99–114. doi: 10.1016/j.molmed.2015.12.006
3. Fomovsky GM, Thomopoulos S, Holmes JW. Contribution of extracellular matrix to the mechanical properties of the heart. *J Mol Cell Cardiol.* 2010;48:490–496. doi: 10.1016/j.yjmcc.2009.08.003
4. Stempien-Otero A, Kim DH, Davis J. Molecular networks underlying myofibroblast fate and fibrosis. *J Mol Cell Cardiol.* 2016;97:153–161. doi: 10.1016/j.yjmcc.2016.05.002
5. Sullivan KE, Quinn KP, Tang KM, Georgakoudi I, Black LD III. Extracellular matrix remodeling following myocardial infarction influences the therapeutic potential of mesenchymal stem cells. *Stem Cell Res Ther.* 2014;5:14. doi: 10.1186/scrt403
6. van Putten S, Shafieyan Y, Hinz B. Mechanical control of cardiac myofibroblasts. *J Mol Cell Cardiol.* 2016;93:133–142. doi: 10.1016/j.yjmcc.2015.11.025
7. Bayomy AF, Bauer M, Qiu Y, Liao R. Regeneration in heart disease-Is ECM the key? *Life Sci.* 2012;91:823–827. doi: 10.1016/j.lfs.2012.08.034
8. Davis J, Burr AR, Davis GF, Birnbaumer L, Molkentin JD. A TRPC6-dependent pathway for myofibroblast transdifferentiation and wound healing in vivo. *Dev Cell.* 2012;23:705–715. doi: 10.1016/j.devcel.2012.08.017

9. Kanisicak O, Khalil H, Ivey MJ, Karch J, Maliken BD, Correll RN, Brody MJ, J Lin SC, Aronow BJ, Tallquist MD, et al. Genetic lineage tracing defines myofibroblast origin and function in the injured heart. *Nat Commun.* 2016;7:12260. doi: 10.1038/ncomms12260
10. Molkentin JD, Bugg D, Ghearing N, Dorn LE, Kim P, Sargent MA, Gunaje J, Otsu K, Davis J. Fibroblast-specific genetic manipulation of p38 mitogen-activated protein kinase in vivo reveals its central regulatory role in fibrosis. *Circulation.* 2017;136:549–561. doi: 10.1161/CIRCULATIONAHA.116.026238
11. Small EM, Thatcher JE, Sutherland LB, Kinoshita H, Gerard RD, Richardson JA, Dimaio JM, Sadek H, Kuwahara K, Olson EN. Myocardin-related transcription factor-a controls myofibroblast activation and fibrosis in response to myocardial infarction. *Circ Res.* 2010;107:294–304. doi: 10.1161/CIRCRESAHA.110.223172
12. Farbehi N, Patrick R, Dorison A, Xaymardan M, Janbandhu V, Wystub-Lis K, Ho JW, Nordon RE, Harvey RP. Single-cell expression profiling reveals dynamic flux of cardiac stromal, vascular and immune cells in health and injury. *Elife.* 2019;8:e43882. doi: 10.7554/eLife.43882
13. Skelly DA, Squiers GT, McLellan MA, Bolisetty MT, Robson P, Rosenthal NA, Pinto AR. Single-cell transcriptional profiling reveals cellular diversity and intercommunication in the mouse heart. *Cell Rep.* 2018;22:600–610. doi: 10.1016/j.celrep.2017.12.072
14. Frangogiannis NG. The extracellular matrix in myocardial injury, repair, and remodeling. *J Clin Invest.* 2017;127:1600–1612. doi: 10.1172/JCI87491
15. Rouillard AD, Holmes JW. Mechanical boundary conditions bias fibroblast invasion in a collagen-fibrin wound model. *Biophys J.* 2014;106:932–943. doi: 10.1016/j.bpj.2013.12.002
16. Turner NA, Porter KE. Function and fate of myofibroblasts after myocardial infarction. *Fibrogenesis Tissue Repair.* 2013;6:5. doi: 10.1186/1755-1536-6-5
17. Dhanjal TS, Lellouche N, von Ruhland CJ, Abehsira G, Edwards DH, Dubois-Randé JL, Moschonas K, Teiger E, Williams AJ, George CH. Massive accumulation of myofibroblasts in the critical isthmus is associated with ventricular tachycardia inducibility in post-infarct swine heart. *JACC Clin Electrophysiol.* 2017;3:703–714. doi: 10.1016/j.jacep.2016.11.010
18. Richardson WJ, Holmes JW. Emergence of collagen orientation heterogeneity in healing infarcts and an agent-based model. *Biophys J.* 2016;110:2266–2277. doi: 10.1016/j.bpj.2016.04.014
19. Goergen CJ, Chen HH, Sakadzic S, Srinivasan VJ, Sosnovik DE. Microstructural characterization of myocardial infarction with optical coherence tractography and two-photon microscopy. *Physiol Rep.* 2016;4:e12894. doi: 10.14814/phy2.12894
20. Muzumdar MD, Tasic B, Miyamichi K, Li L, Luo L. A global double-fluorescent Cre reporter mouse. *Genesis.* 2007;45:593–605. doi: 10.1002/dvg.20335
21. Whittaker P, Boughner DR, Kloner RA. Analysis of healing after myocardial infarction using polarized light microscopy. *Am J Pathol.* 1989;134:879–893.
22. Holmes JW, Borg TK, Covell JW. Structure and mechanics of healing myocardial infarcts. *Annu Rev Biomed Eng.* 2005;7:223–253. doi: 10.1146/annurev.bioeng.7.060804.100453
23. Bredfeldt JS, Liu Y, Conklin MW, Keely PJ, Mackie TR, Eliceiri KW. Automated quantification of aligned collagen for human breast carcinoma prognosis. *J Pathol Inform.* 2014;5:28. doi: 10.4103/2153-3539.139707
24. Bredfeldt JS, Liu Y, Pehlke CA, Conklin MW, Szulczewski JM, Inman DR, Keely PJ, Nowak RD, Mackie TR, Eliceiri KW. Computational segmentation of collagen fibers from second-harmonic generation images of breast cancer. *J Biomed Opt.* 2014;19:16007. doi: 10.1117/1.JBO.19.1.016007
25. Kim P, Yuan A, Nam KH, Jiao A, Kim DH. Fabrication of poly(ethylene glycol): gelatin methacrylate composite nanostructures with tunable stiffness and degradation for vascular tissue engineering. *Biofabrication.* 2014;6:024112. doi: 10.1088/1758-5082/6/2/024112
26. Berry MF, Engler AJ, Woo YJ, Pirolli TJ, Bish LT, Jayasankar V, Morine KJ, Gardner TJ, Discher DE, Sweeney HL. Mesenchymal stem cell injection after myocardial infarction improves myocardial compliance. *Am J Physiol Heart Circ Physiol.* 2006;290:H2196–H2203. doi: 10.1152/ajpheart.01017.2005
27. Hiesinger W, Brukman MJ, McCormick RC, Fitzpatrick JR III, Frederick JR, Yang EC, Muenzer JR, Marotta NA, Berry MF, Atluri P, et al. Myocardial tissue elastic properties determined by atomic force microscopy after stromal cell-derived factor 1α angiogenic therapy for acute myocardial infarction in a murine model. *J Thorac Cardiovasc Surg.* 2012;143:962–966. doi: 10.1016/j.jtcvs.2011.12.028
28. Discher DE, Janmey P, Wang YL. Tissue cells feel and respond to the stiffness of their substrate. *Science.* 2005;310:1139–1143. doi: 10.1126/science.1116995
29. Kim HN, Hong Y, Kim MS, Kim SM, Suh KY. Effect of orientation and density of nanotopography in dermal wound healing. *Biomaterials.* 2012;33:8782–8792. doi: 10.1016/j.biomaterials.2012.08.038
30. Kim DH, Lipke EA, Kim P, Cheong R, Thompson S, Delannoy M, Suh KY, Tung L, Levchenko A. Nanoscale cues regulate the structure and function of macroscopic cardiac tissue constructs. *Proc Natl Acad Sci USA.* 2010;107:565–570. doi: 10.1073/pnas.0906504107
31. Watt FM, Huck WT. Role of the extracellular matrix in regulating stem cell fate. *Nat Rev Mol Cell Biol.* 2013;14:467–473. doi: 10.1038/nrm3620
32. Ray A, Lee O, Win Z, Edwards RM, Alford PW, Kim DH, Provenzano PP. Anisotropic forces from spatially constrained focal adhesions mediate contact guidance directed cell migration. *Nat Commun.* 2017;8:14923. doi: 10.1038/ncomms14923
33. Midwood KS, Schwarzbauer JE. Tenascin-C modulates matrix contraction via focal adhesion kinase- and Rho-mediated signaling pathways. *Mol Biol Cell.* 2002;13:3601–3613. doi: 10.1091/mbc.e02-05-0292
34. Grashoff C, Hoffman BD, Brenner MD, Zhou R, Parsons M, Yang MT, McLean MA, Sligar SG, Chen CS, Ha T, et al. Measuring mechanical tension across vinculin reveals regulation of focal adhesion dynamics. *Nature.* 2010;466:263–266. doi: 10.1038/nature09198
35. LaCroix AS, Lynch AD, Berginski ME, Hoffman BD. Tunable molecular tension sensors reveal extension-based control of vinculin loading. *Elife.* 2018;7:e33927. doi: 10.7554/eLife.33927
36. Xiao Y, Hill MC, Li L, Deshmukh V, Martin TJ, Wang J, Martin JF. Hippo pathway deletion in adult resting cardiac fibroblasts initiates a cell state transition with spontaneous and self-sustaining fibrosis. *Genes Dev.* 2019;33:1491–1505. doi: 10.1101/gad.329763.119
37. Xiao Y, Hill MC, Zhang M, Martin TJ, Morikawa Y, Wang S, Moise AR, Wythe JD, Martin JF. Hippo signaling plays an essential role in cell state transitions during cardiac fibroblast development. *Dev Cell.* 2018;45:153–169.e6. doi: 10.1016/j.devcel.2018.03.019
38. Lin KC, Moroishi T, Meng Z, Jeong HS, Plouffe SW, Sekido Y, Han J, Park HW, Guan KL. Regulation of Hippo pathway transcription factor TEAD by p38 MAPK-induced cytoplasmic translocation. *Nat Cell Biol.* 2017;19:996–1002. doi: 10.1038/ncb3581
39. Lian I, Kim J, Okazawa H, Zhao J, Zhao B, Yu J, Chinnaiyan A, Israel MA, Goldstein LS, Abujarour R, et al. The role of YAP transcription coactivator in regulating stem cell self-renewal and differentiation. *Genes Dev.* 2010;24:1106–1118. doi: 10.1101/gad.1903310
40. Shao DD, Xue W, Krall EB, Bhutkar A, Piccioni F, Wang X, Schinzel AC, Sood S, Rosenbluh J, Kim JW, et al. KRAS and YAP1 converge to regulate EMT and tumor survival. *Cell.* 2014;158:171–184. doi: 10.1016/j.cell.2014.06.004
41. Fomovsky GM, Rouillard AD, Holmes JW. Regional mechanics determine collagen fiber structure in healing myocardial infarcts. *J Mol Cell Cardiol.* 2012;52:1083–1090. doi: 10.1016/j.yjmcc.2012.02.012
42. Rouillard AD, Holmes JW. Mechanical regulation of fibroblast migration and collagen remodelling in healing myocardial infarcts. *J Physiol.* 2012;590:4585–4602. doi: 10.1113/jphysiol.2012.229484
43. Khalil H, Kanisicak O, Prasad V, Correll RN, Fu X, Schips T, Vagnozzi RJ, Liu R, Huynh T, Lee SJ, et al. Fibroblast-specific TGF-β-Smad2/3 signaling underlies cardiac fibrosis. *J Clin Invest.* 2017;127:3770–3783. doi: 10.1172/JCI94753
44. Dobaczewski M, Bujak M, Li N, Gonzalez-Quesada C, Mendoza LH, Wang XF, Frangogiannis NG. Smad3 signaling critically regulates fibroblast phenotype and function in healing myocardial infarction. *Circ Res.* 2010;107:418–428. doi: 10.1161/CIRCRESAHA.109.216101
45. Ali SR, Ranjbarvaziri S, Talkhabi M, Zhao P, Subat A, Hojjat A, Kamran P, Müller AM, Volz KS, Tang Z, et al. Developmental heterogeneity of cardiac fibroblasts does not predict pathological proliferation and activation. *Circ Res.* 2014;115:625–635. doi: 10.1161/CIRCRESAHA.115.303794
46. Hervas A, Ruiz-Sauri A, de Dios E, Forteza MJ, Minana G, Nunez J, Gomez C, Bonanad C, Perez-Sole N, Gavara J, et al. Inhomogeneity of collagen organization within the fibrotic scar after myocardial infarction: results in a swine model and in human samples. *J Anat.* 2016;228:47–58. doi: 10.1111/joa.12395
47. Nam KH, Kim P, Wood DK, Kwon S, Provenzano PP, Kim DH. Multiscale cues drive collective cell migration. *Sci Rep.* 2016;6:29749. doi: 10.1038/srep29749
48. Provenzano PP, Inman DR, Eliceiri KW, Knittel JG, Yan L, Rueden CT, White JG, Keely PJ. Collagen density promotes mammary tumor initiation and progression. *BMC Med.* 2008;6:11. doi: 10.1186/1741-7015-6-11
49. Clarke SA, Richardson WJ, Holmes JW. Modifying the mechanics of healing infarcts: is better the enemy of good? *J Mol Cell Cardiol.* 2016;93:115–124. doi: 10.1016/j.yjmcc.2015.11.028

50. Fu X, Khalil H, Kanisicak O, Boyer JG, Vagnozzi RJ, Maliken BD, Sargent MA, Prasad V, Valiente-Alandi I, Blaxall BC, et al. Specialized fibroblast differentiated states underlie scar formation in the infarcted mouse heart. *J Clin Invest.* 2018;128:2127–2143. doi: 10.1172/JCI98215
51. Arts T, Costa KD, Covell JW, McCulloch AD. Relating myocardial laminar architecture to shear strain and muscle fiber orientation. *Am J Physiol Heart Circ Physiol.* 2001;280:H2222–H2229. doi: 10.1152/ajpheart.2001.280.5.H2222
52. Kim DH, Kshitiz, Smith RR, Kim P, Ahn EH, Kim HN, Marbán E, Suh KY, Levchenko A. Nanopatterned cardiac cell patches promote stem cell niche formation and myocardial regeneration. *Integr Biol (Camb).* 2012;4:1019–1033. doi: 10.1039/c2ib20067h
53. Blaauboer ME, Smit TH, Hanemaaijer R, Stoop R, Everts V. Cyclic mechanical stretch reduces myofibroblast differentiation of primary lung fibroblasts. *Biochem Biophys Res Commun.* 2011;404:23–27. doi: 10.1016/j.bbrc.2010.11.033
54. Hinz B, Mastrangelo D, Iselin CE, Chaponnier C, Gabbiani G. Mechanical tension controls granulation tissue contractile activity and myofibroblast differentiation. *Am J Pathol.* 2001;159:1009–1020. doi: 10.1016/S0002-9440(10)61776-2
55. Mosqueira D, Pagliari S, Uto K, Ebara M, Romanazzo S, Escobedo-Lucea C, Nakanishi J, Taniguchi A, Franzese O, Di Nardo P, et al. Hippo pathway effectors control cardiac progenitor cell fate by acting as dynamic sensors of substrate mechanics and nanostructure. *ACS Nano.* 2014;8:2033–2047. doi: 10.1021/nn4058984
56. Yang C, Tibbitt MW, Basta L, Anseth KS. Mechanical memory and dosing influence stem cell fate. *Nat Mater.* 2014;13:645–652. doi: 10.1038/nmat3889
57. Kim DH, Han K, Gupta K, Kwon KW, Suh KY, Levchenko A. Mechanosensitivity of fibroblast cell shape and movement to anisotropic substratum topography gradients. *Biomaterials.* 2009;30:5433–5444. doi: 10.1016/j.biomaterials.2009.06.042
58. Kim P, Kim DH, Kim B, Choi SK, Lee SH, Khademhosseini A, Langer R, Suh KY. Fabrication of nanostructures of polyethylene glycol for applications to protein adsorption and cell adhesion. *Nanotechnology.* 2005;16:2420–2426. doi: 10.1088/0957-4484/16/10/072
59. Davis J, Salomonis N, Ghearing N, Lin SC, Kwong JQ, Mohan A, Swanson MS, Molkentin JD. MBNL1-mediated regulation of differentiation RNAs promotes myofibroblast transformation and the fibrotic response. *Nat Commun.* 2015;6:10084. doi: 10.1038/ncomms10084
60. Schindelin J, Arganda-Carreras I, Frise E, Kaynig V, Longair M, Pietzsch T, Preibisch S, Rueden C, Saalfeld S, Schmid B, et al. Fiji: an open-source platform for biological-image analysis. *Nat Methods.* 2012;9:676–682. doi: 10.1038/nmeth.2019
61. Püspöki Z, Storath M, Sage D, Unser M. Transforms and operators for directional bioimage analysis: a survey. *Adv Anat Embryol Cell Biol.* 2016;219:69–93. doi: 10.1007/978-3-319-28549-8_3
62. McQuin C, Goodman A, Chernyshev V, Kamentsky L, Cimini BA, Karhohs KW, Doan M, Ding L, Rafelski SM, Thirstrup D, et al. CellProfiler 3.0: next-generation image processing for biology. *PLoS Biol.* 2018;16:e2005970. doi: 10.1371/journal.pbio.2005970
63. Berg S, Kutra D, Kroeger T, Straehle CN, Kausler BX, Haubold C, Schiegg M, Ales J, Beier T, Rudy M, et al. ilastik: interactive machine learning for (bio)image analysis. *Nat Methods.* 2019;16:1226–1232. doi: 10.1038/s41592-019-0582-9